Available online at www.sciencedirect.com
ScienceDirect
Int. J. Electron. Commun. (AEÜ) 64 (2010) 36–46
International Journal AEÜ of Electronics and Communications
www.elsevier.de/aeue

High-frequency asymptotic formulation for prompt response of parabolic reflector antennas

Cássio G. Rego[a,*], Sandro T.M. Gonçalves[b], Fernando J.S. Moreira[a]

[a] *Department of Electronics Engineering, Federal University of Minas Gerais, Belo Horizonte, Minas Gerais, Brazil*
[b] *Federal Center for Technology Education, Divinópolis Unit, Electromechanics Department, Divinópolis, Minas Gerais, Brazil*

Received 3 July 2008; accepted 11 October 2008

Abstract

This work presents some important concepts for the temporal characterization of reflector antennas based on the determination of the transient antenna response together with a useful definition of the early-time antenna radiation pattern. The concepts are useful in the analysis and design of reflector antennas intended for high resolution radars and for high capacity digital, and UWB communication systems.

Keywords: Reflector antennas; High-frequency asymptotic methods; Prompt response; Time-domain analysis; Early-time radiation patterns

1. Introduction

The continuous development of high capacity wireless communication systems and high resolution radars has motivated the investigation of time-domain techniques for the analysis and design of reflector antennas. High data rates employed in modern digital communication systems are generally achieved by modulation schemes associated with phase, frequency, or amplitude keying, which can be distorted by transient effects during the antenna radiation process. In the case of high resolution radars, the analysis of ultra-short pulse radiation based on traditional frequency-domain techniques may be impractical due to the ultra broad operation bandwidth. As a consequence, transient analysis of electromagnetic phenomena has been studied and methods to obtain the field scattered from conducting surfaces have been developed directly in time domain [1–8]. Fortunately, frequency-domain asymptotic techniques such as physical optics (PO) corrected by fringe wave currents (FWCs) and ray tracing methods, like the uniform theory of diffraction (UTD) and the uniform asymptotic theory (UAT), can be transformed to time domain, providing efficient, fast, physically transparent, and very accurate tools to determine transient response of reflector antennas [6–10]. However, it is important to notice that the concepts of gain and radiation pattern as usually proposed in frequency domain may have to be adapted for time-domain analysis [11,12].

The definitions of gain and radiation pattern in time domain were introduced by Farr and Baum [11], based on the concept of norms applied to temporal signals. Using such norms, it is possible to compare the energy (or power) of the radiated field with that of the antenna driving source. In their work, Farr and Baum were interested in the radiation parameters of ultra-short pulse transmitting antennas, whose radiated fields were obtained by a formulation valid in their principal planes only. Later, Shlivinski, Heyman, and Kastner introduced integral operators for the time-domain characterization of a transmitter–receiver short dipole [12]. In that study, energy norms were applied to the radiated field and driving voltage waveforms, allowing the definition of a

* Corresponding author. Tel.: +55 31 3409 4861.
E-mail address: cassio@cpdee.ufmg.br (C.G. Rego).

1434-8411/$ - see front matter © 2008 Elsevier GmbH. All rights reserved.
doi:10.1016/j.aeue.2008.10.002

gain operator which can be expressed as an autocorrelation function and used to determine the transmitting antenna radiation pattern [12].

In the present work, some useful elements for the time-domain characterization of reflector antennas are developed. In Section 2, the integral operators introduced by Shlivinski, Heyman, and Kastner are extended to determine the radiation pattern of reflector antennas. The formulation for the transient radiated fields is obtained by applying a time-domain version of the physical optics (TDPO) corrected by FWCs (TDPO + FWCs), introduced by Rego, Hasselmann, and Moreira [8,9]. The technique is derived from a well-known high-frequency formulation [3,13–15] by means of a Fourier inversion and, therefore, is accurate for early times. The asymptotic nature of such technique makes it suitable to obtain the so-called prompt response of reflector antennas. Case studies concerning a reflector impulse radiating antenna (IRA) and a front-fed paraboloidal reflector illuminated by 4-PSK pulses are presented in Section 3, in order to illustrate the applicability of the concepts that appear herein. Finally, to demonstrate the validity of the present asymptotic formulation, the radiation pattern of a paraboloidal reflector fed by a continuous wave (CW) source is calculated by the TDPO + FWCs technique and compared with a frequency-domain full-wave method of moments (MoM) solution.

2. Prompt response of reflector antennas: PO and FWCs approach

2.1. Early-time radiated field

The electric far field radiated by electric and magnetic current distributions can be expressed as a convolution integral [11,12]

$$\mathbf{E}(\mathbf{r},t) = -\frac{\mu_0}{4\pi r}\mathbf{h}^{\mathrm{t}}(\hat{\mathbf{r}},t) * f(t), \tag{1}$$

where $f(t)$ is the waveform of the driving source, μ_0 is the free-space magnetic permeability, $\mathbf{r} = r\hat{\mathbf{r}}$ locates the observation point, and $\mathbf{h}^{\mathrm{t}}(\hat{\mathbf{r}},t)$ is the effective height of the transmitting antenna [12]. For radiating sources bounded in a volume V', we have

$$\mathbf{h}^{\mathrm{t}}(\hat{\mathbf{r}},t) = \frac{\partial}{\partial t}\int_{V'} \mathbf{J}^{\delta}_{\perp}(\mathbf{r}', t-\tau_0)\,\mathrm{d}V' + \frac{\partial}{\partial t}\int_{V'} \frac{1}{Z_0}\mathbf{M}^{\delta}(\mathbf{r}', t-\tau_0)\times\hat{\mathbf{r}}\,\mathrm{d}V', \tag{2}$$

where Z_0 is the free-space intrinsic impedance, τ_0 is the time spent between the electromagnetic field generation by a source point at $\mathbf{r}'$ and the arrival of the first wavefront at the observation point

$$\tau_0 = \frac{1}{c}(r - \hat{\mathbf{r}}\cdot\mathbf{r}'), \tag{3}$$

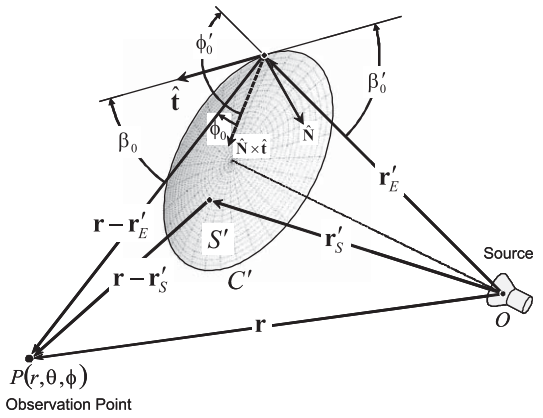

Fig. 1. Geometry for a reflector surface with the vectors and angles employed in the TDPO + FWCs formulation.

and c is the free-space velocity of light. The vectors $\mathbf{J}^{\delta}_{\perp}(\mathbf{r}', t)$ and $\mathbf{M}^{\delta}(\mathbf{r}', t)$ are the source-related electric and magnetic impulsive currents, respectively. In (2) we use a compact notation (hereinafter denoted by the subscript $\perp$) for the vector components which are orthogonal to the direction of propagation $\hat{\mathbf{r}}$:

$$\mathbf{J}^{\delta}_{\perp}(\mathbf{r}', t) = \mathbf{J}^{\delta}(\mathbf{r}', t) - [\mathbf{J}^{\delta}(\mathbf{r}', t)\cdot\hat{\mathbf{r}}]\hat{\mathbf{r}}. \tag{4}$$

For reflector antennas, the TDPO + FWCs method can be applied and the transmitting antenna effective height related to the prompt (early-time) response is given by [8,9]

$$\mathbf{h}^{\mathrm{t}}(\hat{\mathbf{r}},t) = \frac{\partial}{\partial t}\int_{S'} \mathbf{J}^{\delta}_{S_\perp}(\mathbf{r}'_S, t-\tau_S)\,\mathrm{d}S' + \frac{\partial}{\partial t}\int_{C'} \mathbf{I}^{\delta}_{FW_\perp}(\mathbf{r}'_E, t-\tau_E)\,\mathrm{d}\ell' + \frac{\partial}{\partial t}\int_{C'} \frac{1}{Z_0}\mathbf{M}^{\delta}_{FW}(\mathbf{r}'_E, t-\tau_E)\times\hat{\mathbf{r}}\,\mathrm{d}\ell', \tag{5}$$

where S' and C' describe the reflector surface and rim, respectively, whose points are located by the vectors $\mathbf{r}'_S$ and $\mathbf{r}'_E$ (see Fig. 1), $\mathbf{J}^{\delta}_S(\mathbf{r}'_S, t)$ represents the electric PO impulsive current over S', and $\mathbf{I}^{\delta}_{FW}(\mathbf{r}'_E, t)$ and $\mathbf{M}^{\delta}_{FW}(\mathbf{r}'_E, t)$ represent the electric and magnetic FWC impulsive currents at C', respectively. The temporal variables τ_S and τ_E in (5) are given by

$$\tau_S = \frac{1}{c}(r - \hat{\mathbf{r}}\cdot\mathbf{r}'_S), \tag{6}$$

$$\tau_E = \frac{1}{c}(r - \hat{\mathbf{r}}\cdot\mathbf{r}'_E), \tag{7}$$

and denote the time delays related to the propagation from the surface and FWCs to the observation point, respectively. The currents $\mathbf{J}^{\delta}_S(\mathbf{r}'_S, t)$, $\mathbf{I}^{\delta}_{FW}(\mathbf{r}'_E, t)$, and $\mathbf{M}^{\delta}_{FW}(\mathbf{r}'_E, t)$ are obtained from the field incident upon the reflector surface and

are given by [8,9]

$$\mathbf{J}_S^{\delta}(\mathbf{r}'_S, t) = 2\hat{\mathbf{N}} \times \mathbf{H}_i^{\delta}(\mathbf{r}'_S, t), \tag{8a}$$

$$\mathbf{I}_{FW}^{\delta}(\mathbf{r}'_E, t) = \frac{D_e^{I,FW}(\mathbf{r}'_S, \mathbf{r}'_E)}{\mu_0}\hat{\mathbf{t}} \int_{-\infty}^{t} \hat{\mathbf{t}} \cdot \mathbf{E}_i^{\delta}(\mathbf{r}'_E, \tau)\,\mathrm{d}\tau + cD_h^{I,FW}(\mathbf{r}'_S, \mathbf{r}'_E)\hat{\mathbf{t}} \int_{-\infty}^{t} \hat{\mathbf{t}} \cdot \mathbf{H}_i^{\delta}(\mathbf{r}'_E, \tau)\,\mathrm{d}\tau, \tag{8b}$$

$$\mathbf{M}_{FW}^{\delta}(\mathbf{r}'_E, t) = \frac{D_h^{M,FW}(\mathbf{r}'_S, \mathbf{r}'_E)}{\varepsilon_0}\hat{\mathbf{t}} \int_{-\infty}^{t} \hat{\mathbf{t}} \cdot \mathbf{H}_i^{\delta}(\mathbf{r}'_E, \tau)\,\mathrm{d}\tau, \tag{8c}$$

where $\mathbf{E}_i^{\delta}(\mathbf{r}, t)$ and $\mathbf{H}_i^{\delta}(\mathbf{r}, t)$ are the impulse incident fields, ε_0 is the free-space permittivity, $\hat{\mathbf{N}}$ is the surface S' unit normal towards the source, and $\hat{\mathbf{t}}$ is the unit tangent to the reflector rim C'. The coefficients $D_e^{I,FW}(\mathbf{r}'_S, \mathbf{r}'_E)$, $D_h^{I,FW}(\mathbf{r}'_S, \mathbf{r}'_E)$, and $D_h^{M,FW}(\mathbf{r}'_S, \mathbf{r}'_E)$ are given by [8,9]

$$D_e^{I,FW}(\mathbf{r}'_S, \mathbf{r}'_E) = \frac{\sin(\phi'_0/2)}{\sin^2\beta'_0} g(\mathbf{r}'_S, \mathbf{r}'_E), \tag{9a}$$

$$D_h^{I,FW}(\mathbf{r}'_S, \mathbf{r}'_E) = \left\{ \frac{\cot\beta'_0[1 + 2\sin(\alpha_E/2)\cos(\phi'_0/2)]}{\sin\beta'_0 \sin(\alpha_E/2)} - \frac{\cot\beta_0 \cos\phi_0}{\sin\beta'_0 \sin(\alpha_E/2)} \right\} g(\mathbf{r}'_S, \mathbf{r}'_E), \tag{9b}$$

$$D_h^{M,FW}(\mathbf{r}'_S, \mathbf{r}'_E) = \frac{\sin\phi_0}{\sin\beta_0 \sin\beta'_0 \sin(\alpha_E/2)} g(\mathbf{r}'_S, \mathbf{r}'_E), \tag{9c}$$

where

$$g(\mathbf{r}'_S, \mathbf{r}'_E) = \frac{1}{\cos(\phi'_0/2) + \sin(\alpha_E/2)}, \tag{10}$$

$$\alpha_E = \cos^{-1}\left[\frac{\sin\beta_0 \cos\phi_0 + \cot\beta'_0(\cos\beta_0 - \cos\beta'_0)}{\sin\beta'_0}\right]. \tag{11}$$

The angles ϕ'_0, ϕ_0, β'_0, and β_0 which appear in (9a)–(11) and are illustrated in Fig. 1 are unambiguously given by

$$\cos\phi'_0 + \mathrm{j}\sin\phi'_0 = -\frac{\mathbf{r}'_E \cdot (\hat{\mathbf{N}} \times \hat{\mathbf{t}} + \mathrm{j}\hat{\mathbf{N}})}{|\mathbf{r}'_E|\sin\beta'_0}, \tag{12a}$$

$$\cos\phi_0 + \mathrm{j}\sin\phi_0 = -\frac{(\mathbf{r} - \mathbf{r}'_E) \cdot (\hat{\mathbf{N}} \times \hat{\mathbf{t}} + \mathrm{j}\hat{\mathbf{N}})}{|\mathbf{r} - \mathbf{r}'_E|\sin\beta'_0}, \tag{12b}$$

$$\beta'_0 = \cos^{-1}\left(\frac{\mathbf{r}'_E}{|\mathbf{r}'_E|} \cdot \hat{\mathbf{t}}\right), \tag{12c}$$

$$\beta_0 = \cos^{-1}\left(\frac{\mathbf{r} - \mathbf{r}'_E}{|\mathbf{r} - \mathbf{r}'_E|} \cdot \hat{\mathbf{t}}\right). \tag{12d}$$

As in the usual frequency-domain analysis, the application of a temporal version of the FWCs to complement the TDPO surface currents improves the accuracy of the field calculation in the antenna side lobe region. As a consequence, the formulation presented here turns out to be an efficient tool to calculate the time-domain radiated fields for arbitrary aspects of observation [8,9].

2.2. Gain operator and radiation pattern for the antenna transmitting mode

The gain operators for the calculation of transmitting time-domain radiation patterns can be obtained from energy norms of realistic signals. Under this perspective, it is possible to apply an autocorrelation function to calculate the norm of a time-dependent driving signal $f(t)$

$$\|f(t)\|^2 = \mathscr{R}_f(0), \tag{13}$$

where

$$\mathscr{R}_f(\xi) = \int_{-\infty}^{\infty} f(t) f(t - \xi)\,\mathrm{d}t \tag{14}$$

is the autocorrelation function of signal $f(t)$. Using the norm definition (13), Shlivinski, Heyman, and Kastner defined the time-domain transmitting antenna gain operator $\mathbf{g}^{\mathrm{t}}(\hat{\mathbf{r}}, \xi)$ as [12]

$$\frac{1}{Z_0}\mathscr{R}_{\mathbf{E}}(\mathbf{r}, \xi) = \frac{\varepsilon_g}{4\pi r^2}\mathbf{g}^{\mathrm{t}}(\hat{\mathbf{r}}, \xi) * \frac{\mathscr{R}_f(\xi)}{\mathscr{R}_f(0)}, \tag{15}$$

where the operator $*$ represents a time convolution integral, ε_g is the maximum energy available from the driving sources and

$$\mathscr{R}_{\mathbf{E}}(\mathbf{r}, \xi) = \mathscr{R}_{E_\theta}(\mathbf{r}, \xi)\hat{\boldsymbol{\theta}} + \mathscr{R}_{E_\phi}(\mathbf{r}, \xi)\hat{\boldsymbol{\phi}} \tag{16}$$

is the far-field autocorrelation vector composed of the autocorrelation functions of the spherical components E_θ and E_ϕ of the electric field. The definition of the gain operator in (15) has the following frequency-domain counterpart [12]:

$$\frac{1}{2Z_0}|\tilde{\mathbf{E}}(\mathbf{r}, \omega)|^2\hat{\mathbf{p}} = \frac{1}{4\pi r^2}\tilde{\mathbf{g}}^{\mathrm{t}}(\hat{\mathbf{r}}, \omega)\tilde{P}_{\mathrm{in}}(\omega), \tag{17}$$

where $\tilde{\mathbf{E}}(\mathbf{r}, \omega)$ and $\tilde{\mathbf{g}}^{\mathrm{t}}(\hat{\mathbf{r}}, \omega)$ are the radiated electric far field and the transmitting gain vector in frequency domain, respectively, $P_{\mathrm{in}}(\omega)$ is the antenna input power, and the polarization vector $\hat{\mathbf{p}}$ is defined by

$$\hat{\mathbf{p}} = \frac{\tilde{\mathbf{E}}(\mathbf{r}, \omega)}{|\tilde{\mathbf{E}}(\mathbf{r}, \omega)|}. \tag{18}$$

From (1) and (15), an explicit expression was derived for the transmitting antenna gain operator [12]

$$\mathbf{g}^{\mathrm{t}}(\hat{\mathbf{r}}, \xi) = \frac{\mu_0^2}{4\pi\varepsilon_g Z_0}\mathscr{R}_{\mathbf{h}^{\mathrm{t}}}(\hat{\mathbf{r}}, \xi), \tag{19}$$

where $\mathscr{R}_{\mathbf{h}^{\mathrm{t}}}(\hat{\mathbf{r}}, \xi)$ is the autocorrelation vector of the transmitting antenna effective height $\mathbf{h}^{\mathrm{t}}(\hat{\mathbf{r}}, t)$, which is given by (5)

in the present work. The transmitting antenna may be parameterized in terms of a time-independent radiation pattern or energy-gain parameter defined by [12]

$$G^{\mathrm{t}}(\hat{\mathbf{r}}) = \left| \mathbf{g}^{\mathrm{t}}(\hat{\mathbf{r}}, \xi) * \frac{\mathscr{R}_f(\xi)}{\mathscr{R}_f(0)} \right|_{\xi=0}. \tag{20}$$

For example, considering the particular case of a source with a temporal sinusoidal behavior and infinity duration, i.e.,

$$f(t) = A_c \sin \omega_c t, \tag{21}$$

where A_c and ω_c are the source amplitude and angular frequency, respectively, it is possible to employ the autocorrelation function

$$\mathscr{R}_f(\xi) = \lim_{T\to\infty} \frac{1}{2T} \int_{-T}^{T} f(t) f(t-\xi)\,\mathrm{d}t, \tag{22}$$

and use the norm definition (13) to conclude that

$$\|f(t)\|^2 = \mathscr{R}_f(0) = \frac{A_c^2}{2}, \tag{23}$$

as expected. As a consequence, one can show that the time-domain radiation pattern (20) leads into its usual frequency-domain counterpart [12].

3. Case studies

As already pointed out in the previous section, the determination of the antenna time-domain radiation pattern depends on the time behavior of the transmitted signal $f(t)$, which, in turn, depends on the antenna application. In this section, results determined from the time-domain effective height, $\mathbf{h}^{\mathrm{t}}(\hat{\mathbf{r}}, t)$, are obtained for three case studies, all of them involving a paraboloidal reflector antenna depicted in Fig. 2. Co-polar and cross-polar time-independent energy-gain patterns were obtained from $\mathbf{h}^{\mathrm{t}}(\hat{\mathbf{r}}, t)$ according to the third definition of Ludwig [16].

In the first case, the prompt response of an IRA is determined in several observation planes. In the second example, a front-fed paraboloidal reflector antenna is excited with a 4-PSK type signal and its temporal radiation pattern is obtained. In the third case study, the formulation discussed in Section 2 is validated in the analysis of a front-fed paraboloidal reflector illuminated by a CW source, where the time-domain radiation pattern obtained by (20) is compared with a frequency-domain radiation pattern calculated from a full-wave analysis based on the MoM technique. In all case studies, the incident field radiated by the reflector antenna feed will be expressed by the vectors

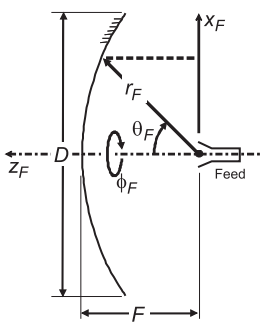

Fig. 2. Geometry of a front-fed paraboloidal reflector.

$$\mathbf{E}_i(\mathbf{r}_F, t) = \frac{f(t - r_F/c)}{r_F} \mathbf{p}(\theta_F, \phi_F), \tag{24}$$

$$\mathbf{H}_i(\mathbf{r}_F, t) = \frac{\hat{\mathbf{r}}_F}{Z_0} \times \mathbf{E}_i(\mathbf{r}_F, t), \tag{25}$$

where $f(t)$ represents the source (signal) temporal behavior and the vector $\mathbf{p}(\theta_F, \phi_F)$ describes its spatial distribution and polarization.

3.1. A reflector IRA prompt response

IRAs generate electromagnetic energy in very short periods of time and have been proposed for different applications [17,18]. The results of this case study will allow us to conclude that the formulation discussed in Section 2 can be employed to perform an intermediate analysis of a reflector IRA. An idealized analysis using a time-domain extension of the aperture method was made by Chou, Pathak, and Rosseau [7]. A practical analysis based on MoM and validated by measurements was recently made by Manteghi and Rahmat-Samii [18]. The TDPO + FWCs technique of Section 2 provides more accuracy than the aperture method of [7], but it is not as accurate as the rigorous MoM solution. However, as the formulation of Section 2 is intended to direct time-domain analysis, it leads to more time-efficient computer algorithm than the usual frequency-domain MoM with a Fourier inversion scheme as performed in [18].

A reflector IRA comprises a paraboloidal reflector fed by a TEM transmission line, which can be described as a Huygen's source [7], with

$$\mathbf{p}(\theta_F, \phi_F) = \hat{\mathbf{r}}_F \times \hat{\mathbf{r}}_F \times \hat{\mathbf{x}}_F + \hat{\mathbf{y}}_F \times \hat{\mathbf{r}}_F, \tag{26}$$

where the unit vectors $\hat{\mathbf{r}}_F$, $\hat{\mathbf{x}}_F$, and $\hat{\mathbf{y}}_F$ correspond to the feed coordinate system illustrated in Fig. 2. The temporal function

$$f(t) = -\frac{4V_0 t}{T^2} \exp\left(-\frac{2t^2}{T^2}\right) \tag{27}$$

adopted here describes an input differentiated Gaussian pulse [18], where V_0 is a normalization constant and T is related to the pulse width. In the present study $T = 1$ ns.

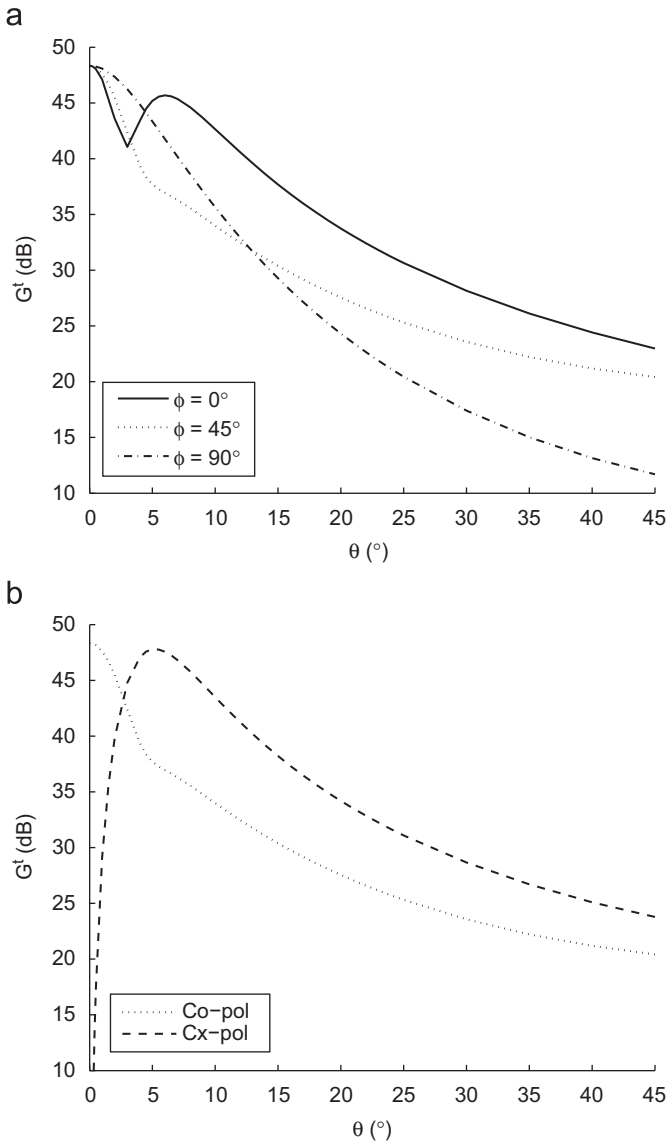

Fig. 3. Time-domain radiation patterns of a paraboloidal reflector IRA with $D = 7.5\,\text{m}$ and $F = 0.4D$. (a) Co-polar patterns and (b) co- and cross-polar patterns at plane $\phi = 45^\circ$.

Fig. 3 shows the time-domain energy gain pattern of a paraboloidal reflector IRA with diameter $D = 7.5\,\text{m}$ and focal distance $F = 0.4D$, observed at planes $\phi = 0^\circ$, 45°, and 90° for elevation angles in the range $0^\circ < \theta < 45^\circ$. These results, obtained from (20) with the help of (5)–(12) and (19), show that the energy contained in the radiated pulse is mainly directed toward boresight (θ=0°), as expected. However, the side lobe levels are greater than those generally observed in a narrow band (i.e., frequency domain) operation. Such behavior cannot be easily observed in a frequency-domain analysis, where power radiation patterns are individually obtained for each frequency. This observation depicts the usefulness and applicability of the formulation discussed in Section 2.

The paraboloidal reflector IRA transient response at plane $\phi = 0^\circ$ and for observation points close to and far from boresight are shown in Fig. 4, where T_0 is the time of arrival of the first wavefront on the observation point (4000 m away from the antenna focus). From Fig. 4(a), it is possible to observe the desired impulse-like behavior of the radiated field near boresight. The high-frequency asymptotic nature of the prompt response is evident in the results presented in Fig. 4(a), because of the absence of pulse tails (i.e., late-time field), related to source low-frequency components and the reflector external natural resonances [19,20]. Diffraction effects from the reflector rim are more pronounced at observation points in the side lobe region. Consequently, the scattered pulses depicted in Fig. 4(b) present time dispersion.

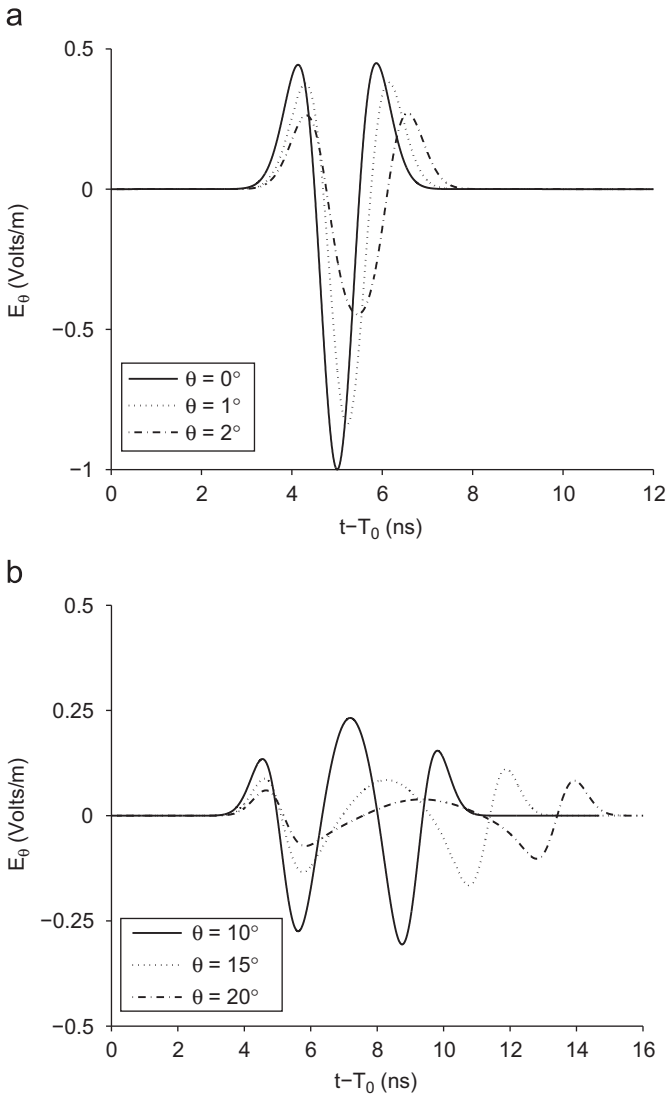

Fig. 4. Transient response of a reflector IRA at plane $\phi = 0°$. (a) Boresight region and (b) side lobe region.

3.2. Radiation pattern of digital communication reflector antennas

In this application, the feed of the front-fed paraboloidal antenna is modeled as a x-polarized raised cosine [21]

$$\mathbf{p}(\theta_F, \phi_F) = \cos^n \theta_F (\cos\ \phi_F \hat{\boldsymbol{\theta}}_F - \sin\ \phi_F \hat{\boldsymbol{\phi}}_F), \tag{28}$$

where $n = 1$ in the present work and the unit vectors $\hat{\boldsymbol{\theta}}_F$ and $\hat{\boldsymbol{\phi}}_F$ are referred to the feed spherical coordinate system depicted in Fig. 2. Considering the transmission of a 4-PSK signal at rate R_b, it is possible to represent a M bit data vector by

$$f(t) = A_c \sum_{n=0}^{M} \left\{ \sin\left(\omega_c t - \varepsilon_n \frac{\pi}{4}\right) \times [U(t - nT_b) - U(t - (n+1)T_b)] \right\}, \tag{29}$$

where A_c is a constant amplitude, ω_c is the carrier angular frequency, T_b is the bit duration ($T_b = 1/R_b$), $U(t)$ is the Heaviside unit step function, and

$$\varepsilon_n = \begin{cases} 1 & \text{for each pair of bits 11,} \\ 3 & \text{for each pair of bits 01,} \\ 5 & \text{for each pair of bits 00,} \\ 7 & \text{for each pair of bits 10.} \end{cases} \tag{30}$$

A paraboloidal reflector antenna with $D = 100\lambda_c$ (where λ_c is the carrier wavelength) and $F = 0.4D$ was analyzed. The point source at the reflector focus radiates a field with temporal behavior described by (24), (25) and (28)–(30), for which the values $M = 4$ and $\varepsilon_n = \{1, 3, 5, 7\}$ were used. Fig. 5 shows the energy gain pattern given by (20) at planes $\phi = 0°$ and 45° (where the cross-polar pattern reach its maximum) for 4-PSK signals with two different bit rates: $T_b = 5T_c$

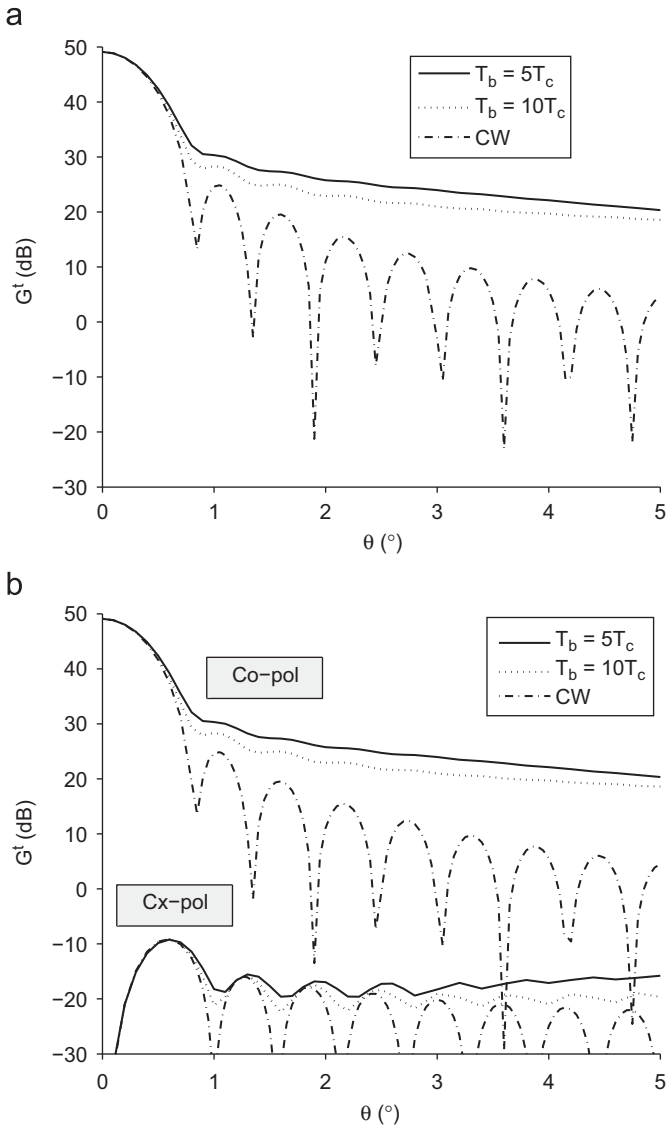

Fig. 5. Time-domain radiation patterns of a paraboloidal reflector illuminated by a 4-PSK pulse. (a) Co-polar patterns at plane $\phi = 0^\circ$ and (b) co- and cross-polar patterns at plane $\phi = 45^\circ$.

and $10T_c$, where T_c is the carrier period. For comparison purposes, the radiation pattern for a CW signal (with the same frequency of the 4-PSK carrier) is also shown. From inspection of Fig. 5 one observes that the side lobe levels corresponding to the pulsed 4-PSK signals (transmitted as a time-limited data streams) are greater than those observed for the CW signal, as already observed for the reflector IRA, and increase with the bit rate R_b.

The temporal electric field for $T_b = 5T_c$ at the plane $\phi = 0^\circ$ is illustrated in Fig. 6 for observations at $\theta = 0^\circ$, 0.3°, and 1°. For comparison purposes, the CW radiation is also shown. It can be observed from Fig. 6(a) that there are no appreciable transient effects at $\theta = 0^\circ$, as expected. As the observation angle θ increases, transitions between different PSK phases are observed [22]. Comparing these results to those obtained by a CW radiation, it is possible to observe from Fig. 6 the distortion in the amplitude level caused by transient effects with increasing θ, which leads to greater side lobe levels as observed in Fig. 5. In the same way as happened in the previous case study, there is no pulse tails in the 4-PSK pulse transient response, and, this fact shows the limitations of the prompt response introduced here.

3.3. Validation: TDPO + FWCs compared with the MoM

The formulation discussed in Section 2 was derived from a frequency-domain asymptotic theory and is valid for early-time analysis, in principle. In order to validate the theory of Section 2, the time-domain radiation pattern (20) of a front-fed paraboloidal reflector illuminated by a CW point

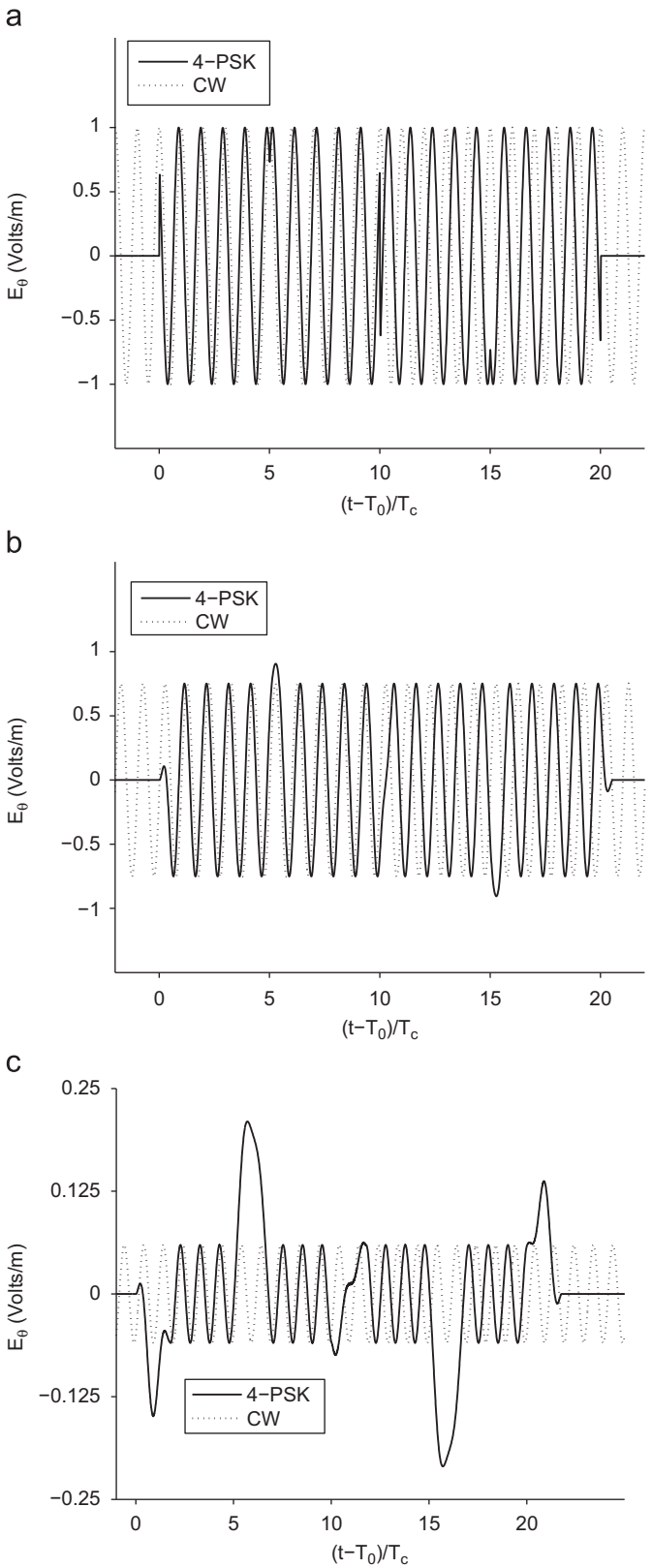

Fig. 6. Transient response for the paraboloidal reflector illuminated by a 4-PSK pulse. (a) $\theta = 0^\circ$, (b) $\theta = 0.3^\circ$ and (c) $\theta = 1^\circ$.

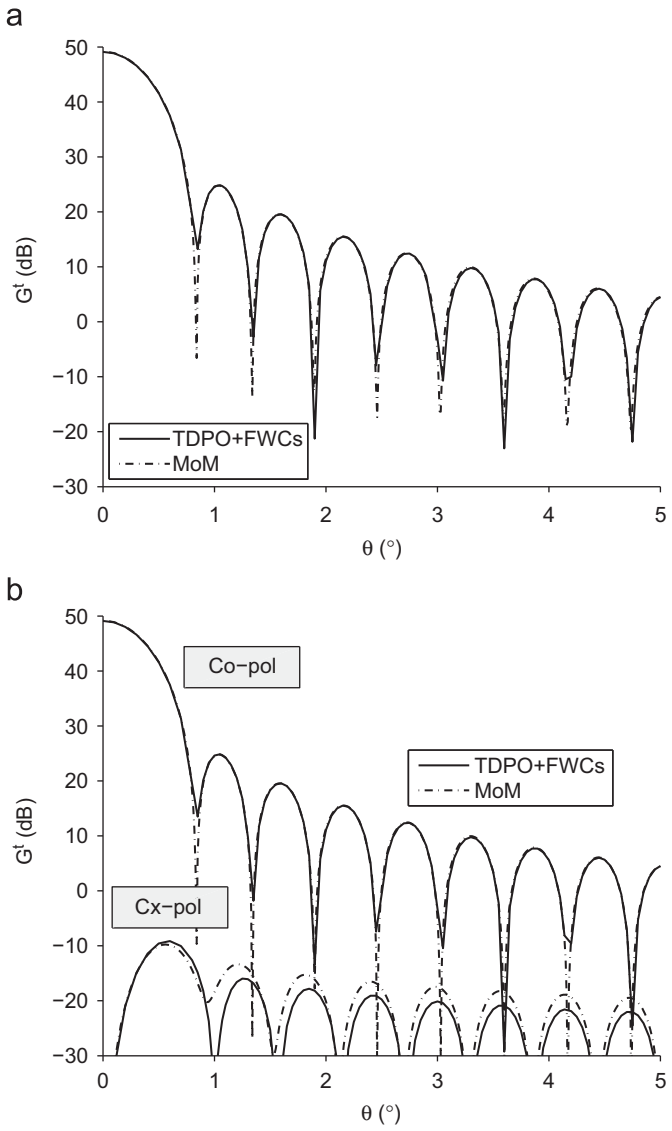

Fig. 7. Validation: TDPO + FWCs and MoM comparison for a paraboloidal antenna excited by a CW source. (a) Co-polar patterns at $\phi = 0^\circ$ and (b) co- and cross-polar patterns at plane $\phi = 45^\circ$.

source is compared to the radiation pattern obtained from a frequency-domain full-wave MoM analysis. The antenna feed is modeled as the raised cosine of (28) with $n = 1$. The signal $f(t)$ is given by (21). The paraboloidal reflector has $D = 100\lambda_c$ and $F = 0.4D$, where λ_c is the carrier wavelength. Fig. 7 depicts the co- and cross-polar radiation patterns at planes $\phi = 0^\circ$ and 45° obtained from the TDPO + FWCs and MoM approaches, illustrating the accuracy of the TDPO + FWC technique employed here.

4. Conclusions

A formulation based on time-domain physical optics corrected by fringe wave currents (TDPO + FWCs) was employed to extend the integral operators developed by Shlivinski, Heyman and Kastner to the broad-band characterization of reflector antennas. The high-frequency asymptotic nature of TDPO + FWCs provides the prompt response and, consequently, the time-domain radiation pattern of reflector antennas, which are accurate for the so-called early times. Such extension allows the analysis of transient response of reflector antennas intended to UWB applications and high-rate digital communication systems, taking into account the distortion of the information-bearing signal caused by diffraction effects.

The applicability and accuracy of the TDPO + FWCs technique were verified by three case studies comprising the analysis of an impulse response antenna (IRA), a communication systems paraboloidal reflector, and a continuous-wave radiation by a front-fed paraboloidal reflector. For the last case, the temporal radiation pattern obtained by the

TDPO + FWCs was compared to a reference solution based on the frequency-domain method of moments with very good agreement between them.

Acknowledgments

This work was partially supported by FAPEMIG (under Project TEC 794/06) and CAPES (under PROCAD 0377058).

References

[1] Felsen LB. Diffraction of a pulse field from an arbitrarily oriented electric or magnetic dipole by a perfectly conducting wedge. SIAM Journal on Applied Mathematics 1974;26(2):306–12.
[2] Veruttipong TW. Time domain version of the uniform GTD. IEEE Transactions on Antennas and Propagation 1990;38(11):1757–64.
[3] Sun E-Y, Rusch WVT. Time-domain physical-optics. IEEE Transactions on Antennas and Propagation 1994;42(1):9–15.
[4] Ianconescu R, Heyman E. Pulse field diffraction by a perfectly conducting wedge: a spectral theory of transients analysis. IEEE Transactions on Antennas and Propagation 1994;42(6):781–9.
[5] Rosseau PR, Pathak PH. Time-domain uniform geometrical theory of diffraction for a curved wedge. IEEE Transactions on Antennas and Propagation 1995;43(12):1375–82.
[6] Sun E-Y. Transient analysis of large paraboloidal reflector antennas. IEEE Transactions on Antennas and Propagation 1995;43(12):1491–6.
[7] Chou H-T, Pathak PH, Rosseau PR. Analytical solution for early-time transient radiation from pulse-excited parabolic reflector antennas. IEEE Transactions on Antennas and Propagation 1997;45(5):829–36.
[8] Rego CG, Hasselmann FJV, Moreira FJS. Time-domain analysis of a reflector antenna illuminated by a Gaussian pulse. Journal of Microwaves and Optoelectronics 1999;1(1):20–8.
[9] Rego CG, Hasselmann FJV. Time-domain equivalent edge currents for the analysis of pulse-excited reflector antennas. Journal of Communication and Information Systems 2006;21(1):15–29 (in Portuguese).
[10] Rego CG, Hasselmann FJV. Time-domain analysis of pulse-excited reflector antennas-UAT approach, In: Proceedings of IEEE Antennas and Propagation Society International Symposium, Boston, MA, USA; July 2001. p. 376–9.
[11] Farr EG, Baum CE. Extending the definitions of antenna gain and radiation pattern into the time domain. Sensor and Simulation Notes, November 1992 (note 350).
[12] Shlivinski A, Heyman E, Kastner R. Antenna characterization in the time domain. IEEE Transactions on Antennas and Propagation 1997;45(7):1140–9.
[13] Michaeli A. Equivalent edge currents for arbitrary aspects of observation. IEEE Transactions on Antennas and Propagation 1984;32(3):252–8.
[14] Michaeli A. Correction to "Equivalent edge currents for arbitrary aspects of observation". IEEE Transactions on Antennas and Propagation 1985;33(2):227.
[15] Michaeli A. Elimination of infinities in equivalent edge currents, part I: fringe current components. IEEE Transactions on Antennas and Propagation 1986;34(7):912–8.
[16] Ludwig AC. The definition of cross polarization. IEEE Transactions on Antennas and Propagation 1973;21(1): 116–9.
[17] Farr EG, Baum CE. Impulse radiating antennas. In: Bertoni HL, Carin L, Felsen LB, editors. Ultra-wideband short pulse electromagnetics. New York: Plenum Press; 1994. p. 139–47.
[18] Manteghi M, Rahmat-Samii Y. On the characterization of a reflector impulse radiating antenna (IRA): full-wave analysis and measured results. IEEE Transactions on Antennas and Propagation 2006;54(3):812–22.
[19] Baum CE, On the singularity expansion method for the solution of electromagnetic interaction problems. AFWL Interaction Notes, December 1971 (note 88).
[20] Morgan MA. Singularity expansion representations of fields and currents in transient scattering. IEEE Transactions on Antennas and Propagation 1984;32(5):466–73.
[21] Balanis CA. Antenna theory: analysis and design. 3rd ed., Hoboken, NJ: Wiley; 2005 p. 913–4.
[22] Sun E-Y. Transient analysis of large paraboloidal reflector antennas. IEEE Transactions on Antennas and Propagation 1995;43(12):1491–6.

Cássio Gonçalves do Rego was born in São Paulo, Brazil, in 1964. He received the B.S. degree in Electrical Engineering from the Universidade de Brasília, Brasília, Brazil, in 1988, and the Master and Doctor degrees in Electrical Engineering from the Catholic University of Rio de Janeiro, Rio de Janeiro, Brazil, in 1991 and 2001, respectively. From 1992 to 1997 he was an Associate Professor at the Electronics and Telecommunications Department of the Catholic University of Minas Gerais, Belo Horizonte, Brazil. Since 1997 he has been with the Electronic Engineering Department of Federal University of Minas Gerais, Belo Horizonte, Brazil. His research interests are in the areas of EM scattering, antennas and radiowave propagation.

Sandro Trindade Mordente Gonçalves was born in Minas Gerais, Brazil, in 1980. He received the B.S. and Master degrees in Electrical Engineering from the Federal University of Minas Gerais, Belo Horizonte, Brazil, in 2003 and 2005, respectively. Since 2006 he has been with the Electromechanics Department of Federal Center for Technological Education of Minas Gerais, Campus V, Divinópolis, Brazil. Currently he is pursuing the Doctor degree in Electrical Engineering at Federal University of Minas Gerais, Belo Horizonte, Brazil, and his main research interests are in the antenna and radiowave propagation field.

Fernando José da Silva Moreira was born in Rio de Janeiro, Brazil, in 1967. He received the B.S. and M.S. degrees in Electrical Engineering from the Catholic University, Rio de Janeiro, Brazil, in 1989 and 1992, respectively, and the Ph.D. degree in Electrical Engineering from the University of Southern California in 1997. Since 1998, he has been with the Department of Electronics Engineering of the Federal University of Minas Gerais, Brazil, where he is currently an Associate Professor. His research interests are in the areas of electromagnetics, antennas, and propagation. He has authored or co-authored over 90 journal and conference papers in these areas. He is a member of Eta Kappa Nu, IEEE Antennas and Propagation Society, and the Brazilian Microwave and Optoelectronics Society.